Available online at www.sciencedirect.com
SCIENCE DIRECT®
Chaos, Solitons and Fractals 29 (2006) 1219–1228
CHAOS SOLITONS & FRACTALS
www.elsevier.com/locate/chaos

Nonlinear dynamics of regenerative cutting processes—Comparison of two models

X.S. Wang [a,*], J. Hu [b], J.B. Gao [b]

[a] Department of Mechanical Engineering, Southeast University, Nanjing 210096, PR China
[b] Department of Electrical and Computer Engineering, University of Florida, Gainesville, FL 32611, USA

Accepted 24 August 2005

Abstract

Understanding the nonlinear dynamics of cutting processes is essential for the improvement of machining technology. We study machine cutting processes by two different models, one has been recently introduced by Litak [Litak G. Chaotic vibrations in a regenerative cutting process. Chaos, Solitons & Fractals 2002;13:1531–5] and the other is the classic delay differential equation model. Although chaotic solutions have been found in both models, well known routes to chaos, such as period-doubling or quasi-periodic motion to chaos are not observed in either model. Careful analysis shows that the chaotic motion from the Litak's model has sharper spectral peaks, a smaller correlation dimension and a smaller value for the largest positive Lyapunov exponent. Implications to the control of chaos in cutting processes are discussed.

1. Introduction

Undesired relative vibrations between the tool and the workpiece may severely degrade the quality of machined surfaces during a cutting process. Effective control of the periodic and chaotic vibrations in all acceptable working conditions is of key importance to machining technology. An important first step toward this goal is to understand the nonlinear dynamics of cutting processes. Since the 1980s, this issue has attracted a lot of attention, and a number of different models describing machining processes have been proposed and analyzed [1–23].

In this paper, we critically analyze two models for describing cutting processes. One is the classic delay differential equation model; the other has been recently introduced by Litak [10]. In the latter model (see Section 2.1), the position of the workpiece in the previous revolution is modelled by a sinusoidal function. We shall argue in the paper that such a sinusoidal function should be interpreted as a harmonic forcing instead of the position of the workpiece in the previous revolution—were the latter true, then the model should not have produced any type of quasi-periodic or chaotic motions claimed in [10], since those motions are not compatible with the simple harmonic processes assumed. By interpreting the position of the workpiece in the previous revolution as a harmonic forcing, one not only eliminates such an in-compatibility, but also may gain some interesting insights into the controlling of complex vibrations of cutting

* Corresponding author.
E-mail addresses: xswang@seu.edu.cn (X.S. Wang), jinghu@ufl.edu (J. Hu), gao@ece.ufl.edu (J.B. Gao).

0960-0779/$ - see front matter © 2005 Elsevier Ltd. All rights reserved.
doi:10.1016/j.chaos.2005.08.131

processes. Such reasoning motivates us to carefully examine the periodic as well as chaotic vibrations in the two models, and make critical comparisons. While we do not observe well-known routes to chaos such as period-doubling or quasi-periodic motions to chaos in either model, we find that before chaos occurs, the motion in both models becomes period-7. Furthermore, it is found that the chaotic motion from the Litak's model has sharper spectral peaks, a smaller correlation dimension and a smaller value for the largest positive Lyapunov exponent. It thus seems that replacing the position of the workpiece in the previous revolution by a harmonic forcing is quite effective in reducing the degree of chaos in cutting processes.

The remainder of the paper is organized as follows. In Section 2, we briefly describe the two models, present analyses of the dynamics of the two models, and make comparisons. Some concluding remarks are discussed in Section 3.

2. Periodic and chaotic vibrations in machine cutting processes

In this section, we analyze the two models describing orthogonal continuous turning processes, as schematized in Fig. 1. Here k denotes the effective spring of a workpiece, c is the damping coefficient, h_0 is the assumed cutting depth while h is the actual one. Ω_0 is a rotational velocity and v_0 is a relative velocity between the tool and the workpiece tangent to the workpiece surface ($v_0 = \Omega_0 r$, where r is the radius of the workpiece). The horizontal displacement of the workpiece symmetry axis at the time t and $t - T$ are denoted by $y(t)$ and $y(t - T)$, respectively, where T is the period of revolution. After the first pass of the tool, the actual cutting depth can be expressed as

$$h(t) = h_0 - y(t) + y(t - T) \tag{1}$$

Below, we briefly describe the two models describing the cutting process, study their dynamics, and make careful comparisons.

2.1. Brief description of the two models

A general delay differential equation model can be casted as [10]

$$\ddot{y}(t) + 2n\dot{y}(t) + p^2 y(t) = \frac{\alpha}{M}[F_y(y(t - T) - y(t) + h_0) - F_y(h_0)] \tag{2}$$

where p is the natural frequency of the free vibration, M is the effective mass of a workpiece, $2n = c/M$ is a damping coefficient, and α is a sign function, $\alpha = \mathrm{sgn}(v_0 - \dot{y}(t))$. F_y is the thrust force, a horizontal component of a nonlinear cutting force. When there is no contact loss, $\alpha = 1$. When contact loss occurs, one has to introduce the following equation:

$$\dot{y}(t^+) = -\beta \dot{y}(t^-) \tag{3}$$

where β is the restitution parameter, t^- and t^+ denotes the time before and after impacts, respectively. When F_y is a linear function, then Eq. (2) is simplified to be [13]

$$\ddot{y}(t) + 2n\dot{y}(t) + p^2 y(t) = C[y(t - T) - y(t)] \tag{4}$$

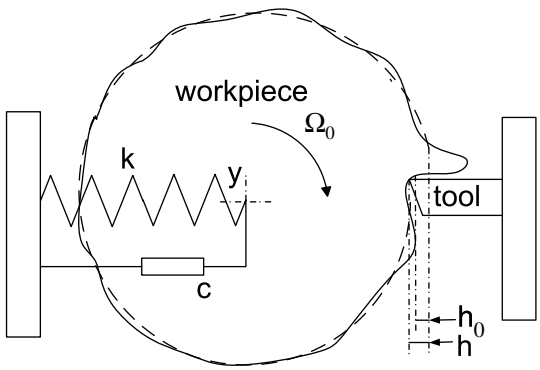

Fig. 1. The model of an orthogonal continuous turning process.

here C is a coefficient. In this paper, we will not adopt a linear functional form for F_y. Instead, we shall follow Litak [10] and use the following relation for F_y:

$$F_y(h) = \Theta(h) K w h^{\frac{3}{4}} \tag{5}$$

where K denotes the cutting resistance, w is a chip width and Θ is the heaviside step function. Eqs. (1)–(3) and (5) constitute our delay differential equation model.

Next let us describe the Litak's model [10]. In his model, $y(t - T)$ is approximated by a sinusoidal function,

$$y(t - T) = a\cos(\omega t - \phi) \tag{6}$$

where ω, a and ϕ are the frequency, amplitude and phase of a surface shape modulation, respectively. Here, ω is the bifurcation parameter. Eqs. (1)–(3), (5) and (6) describe the Litak's model. Because of Eq. (6), this model is no longer a delay differential equation model, but simply an ordinary differential equation model with a time-varying term. Note that if $y(t - T)$ could indeed be a periodic function, then $y(t)$ should also be so. In other words, more complicated motions for $y(t)$, such as chaos, could not occur. But as we shall show below, $y(t)$ can be chaotic. We shall argue that when this occurs, the sinusoidal term be better interpreted as a periodic forcing.

The following system parameters are chosen for both the delay differential equation model and the Litak's model: $K = 1.25 \times 10^9$ N/m^2, $w = 3.0 \times 10^{-3}$ m, $h_0 = 0.3 \times 10^{-3}$ m, $p = 816$ rad/s, $M = 17.2$ kg, $a = 0.2 \times 10^{-3}$ m, $\phi = \pi/2$, $\beta = 0.75$ and a relatively small damping $n = 4.3$ s^{-1}. We shall focus on the analysis of the actual cutting depth $h(t)$ time series.

2.2. Analysis of the delay differential equation model

In Fig. 2 we show the time course of the cutting depth $h(t)$ (obtained by Eqs. (1)–(3) and (5)) for four different delay time T. The time series is sampled with $\delta t = 10^{-4}$. The negative value of h means that the tool loses a contact with the workpiece. We notice from Fig. 2(a) that when $T = 1.0$ ms, the cutting process is very smooth with only negligible oscillations around the assumed cutting depth h_0. With the increase of the delay time T, the amplitude of the fluctuation of the cutting depth becomes larger, but it still looks like a periodic motion, as shown in Fig. 2(b) with $T = 1.8$ ms. As the

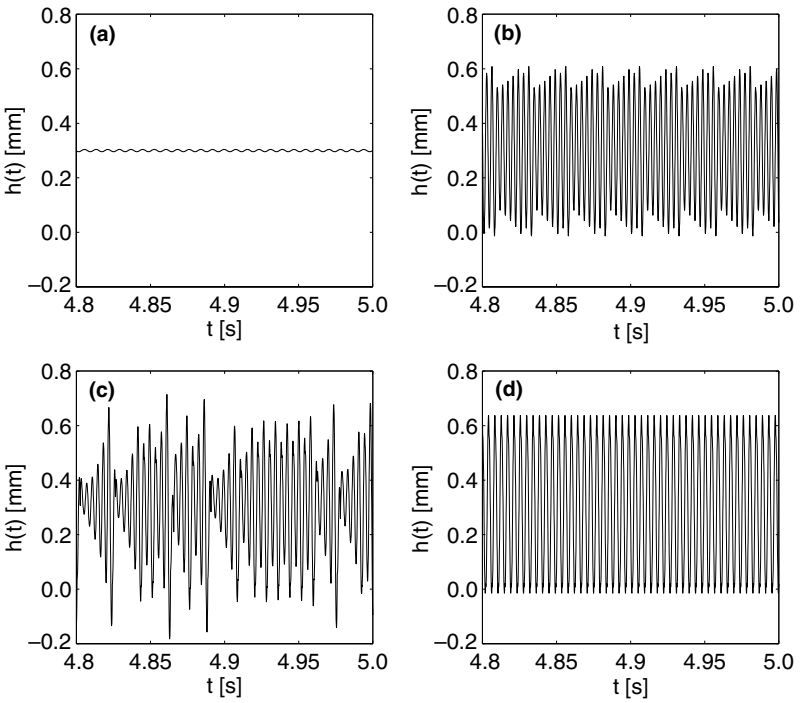

Fig. 2. The actual cutting depth $h(t)$ for various delay time T of the delay differential equation model: (a) $T = 1.0$ ms, (b) $T = 1.8$ ms, (c) $T = 2.1$ ms, (d) $T = 2.3$ ms. The sampling time is $\delta t = 10^{-4}$.

delay T further increases, e.g. $T = 2.1$ ms, the vibration of the cutting depth $h(t)$ becomes aperiodic. Finally when $T = 2.3$ ms, the vibration of the cutting depth changes back to be regular, as shown in Fig. 2(d).

Since the time series shown in Fig. 2(a) and (d) are simple, we shall leave them aside and only focus on the time series shown in Fig. 2(b) and (c). We analyze them by plotting $h(t + L)$ vs. $h(t)$. L is chosen to be 9, in unit of the sample points. As we shall see shortly, such plots can be considered as projection of a reconstructed phase space onto two-dimension. L is chosen such that the structure shown in the figure spreads out fairly evenly and can be clearly seen. For simplicity, we call such plots phase diagrams. They are shown in Fig. 3(a) and (c) for the time series of Fig. 2(b) and (c). The power spectral density (PSD) for the two time series are shown in Fig. 3(b) and (d). We observe from Fig. 3(a) that the orbit in the phase space takes seven runs until the path repeats. We also observe that the smallest spectral peak is 1/7 of the dominant peak in Fig. 3(b). Therefore, the motion for $T = 1.8$ ms is period-7. The phase diagram and PSD for the motion for $T = 2.1$ ms, however, strongly suggest that the time series shown in Fig. 2(c) is chaotic. Below, we employ two different measures to validate this intuition.

To show that the time series is indeed chaotic, first we employ the direct dynamical test for deterministic chaos developed in [24]. This is one of the most stringent tests for chaos developed so far, and has found numerous applications in the study of the effects of noise on dynamical systems [25], estimation of the strength of measurement noise in experimental data [26,27], nature of sea clutter [28], pathological tremors [29], dynamics of Internet transport protocols [30], shear-thickening surfactant solutions [31], dilute sheared aqueous solutions [32], and serrated plastic flows [33]. To employ Gao and Zheng's method [24], we first construct vectors of the form:

$$V_i = [h(i), h(i + L), \ldots, h(i + (m - 1)L)] \tag{7}$$

where m is the embedding dimension and L the delay time. One then computes the following $\Lambda(k)$ curves

$$\Lambda(k) = \left\langle \ln\left(\frac{\|V_{i+k} - V_{j+k}\|}{\|V_i - V_j\|}\right)\right\rangle \tag{8}$$

with $r \leqslant \|V_i - V_j\| \leqslant r + \Delta r$, where r and Δr are prescribed small distances. The angle brackets denote the ensemble average of all possible (V_i, V_j) pairs. The integer k, called the evolution time, corresponds to time $k\delta t$, where δt is

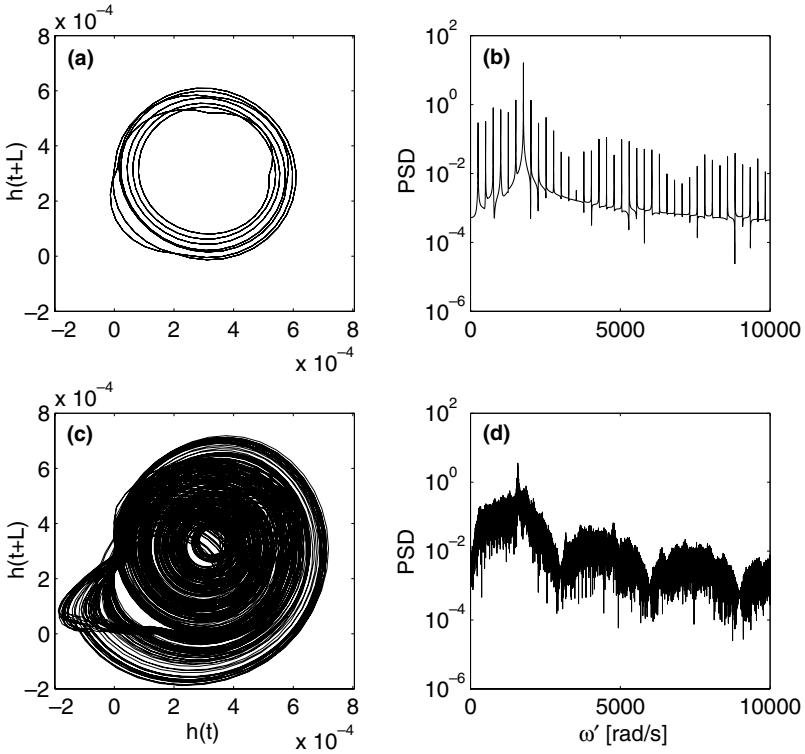

Fig. 3. The phase diagram (a) and (c) and PSD (b) and (d) for the time series of Fig. 2(b) and (c). L in (a) and (c) is chosen to be 9.

the sampling time. Note that geometrically $(r, r+\Delta r)$ defines a shell. The computation is typically carried out for a sequence of shells. For true low-dimensional chaotic systems, the $\Lambda(k)$ curves for different shells form a common envelope, and the largest positive Lyapunov exponent can be objectively estimated by the slope of the envelope. For random systems, the $\Lambda(k)$ curves corresponding to different shells will not form a common envelope, and hence, the system under study will not be interpreted as chaos.

At least two optimal embedding procedures have been proposed. One is a dynamic method introduced by Gao and Zheng [24]; the other is the so-called false nearest neighbor method [34]. It has been found that these two methods yield very similar results. Here we employ the optimal embedding procedure developed in [24]. It is found that a proper L under the given sampling time is 3. Note that this L is much smaller than that used for plotting the phase diagrams (Fig. 3(a) and (c)). This is due to the fact that here the embedding dimension is much larger than 2. The $\Lambda(k)$ curves are found to be quite independent of the embedding dimension m, so long as m is not too small. One example is shown in Fig. 4(a), for the $h(t)$ time series of Fig. 2(c), where the four curves, from bottom to top, correspond to the shells of sizes $(2^{-(i+1)/2}, 2^{-i/2})$, $i = 8, 9, 10, 11$. We observe a common envelope at the lower left corner of Fig. 4(a). The estimated largest positive Lyapunov exponent is 150 bits per sec, or 0.593 bits per cycle of the oscillation, after being multiplied by the period of the oscillation (which is estimated as the reciprocal of the dominant peak in the PSD of Fig. 3).

Next, let us examine the correlation dimension D_2 for the $h(t)$ time series for $T = 2.1$ ms. Correlation dimension is the most commonly used dimension to characterize a chaotic system. D_2 is defined by [35],

$$D_2 = \lim_{\epsilon \to 0} \log C(\epsilon) / \log \epsilon \tag{9}$$

where

$$C(\epsilon) = \frac{1}{N^2} \sum_{i,j=1}^{N} \Theta(\epsilon - ||V_i - V_j||) \tag{10}$$

Θ is the Heaviside step function, V_i and V_j are the vectors reconstructed from the $h(t)$ time series using the same procedure described by Eq. (7), N is the number of points in the time series, and ϵ is a prescribed small distance. As in the calculation of the $\Lambda(k)$ curves, we again use $N = 20{,}000$ and $L = 3$. Fig. 5(a) shows $D_2(\epsilon)$ vs. the scale $\log_2\epsilon$ for a number of m, where $D_2(\epsilon)$ is defined as

$$D_2(\epsilon) = \frac{\log_2 C(\epsilon_{i-1}) - \log_2 C(\epsilon_{i+1})}{\log_2 \epsilon_{i-1} - \log_2 \epsilon_{i+1}} \tag{11}$$

We observe a well-defined plateau. It is worth noting that the $D_2(\epsilon)$ vs. $\log_2\epsilon$ curves for other m, so long as m is not too small, all collapse onto the plateau. Hence, the correlation dimension is $D_2 = 2.35$.

2.3. Analysis of the Litak's model

Now let us analyze the dynamical behaviors of the Litak's model [10]. Fig. 6 shows the $h(t)$ time series (obtained using Eqs. (1)–(3), (5) and (6)) for eight different frequencies ω in increasing order. Note that the time series shown in Fig. 6(a), (e), (g) and (h) were analyzed by Litak by calculating PSD. The time series is sampled with $\delta t = 10^{-6}$ (we

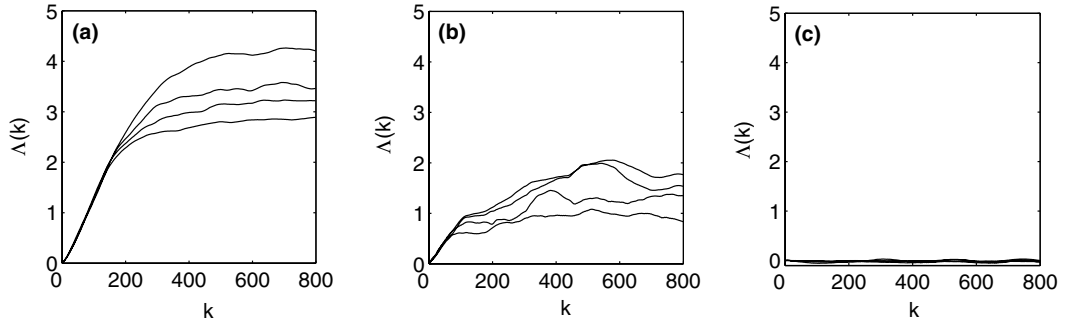

Fig. 4. The $\Lambda(k)$ curves for (a) the chaotic $h(t)$ time series from the delay differential equation model (Fig. 2(c)), (b) the $h(t)$ time series (sampled with 10^{-4}) of Fig. 6(e), and (c) the $h(t)$ time series (sampled with 10^{-4}) of Fig. 6(d). Based on the optimal embedding procedure of [24], L is chosen to be 3 for (a) and 6 for (b) and (c). The curves are fairly independent of m.

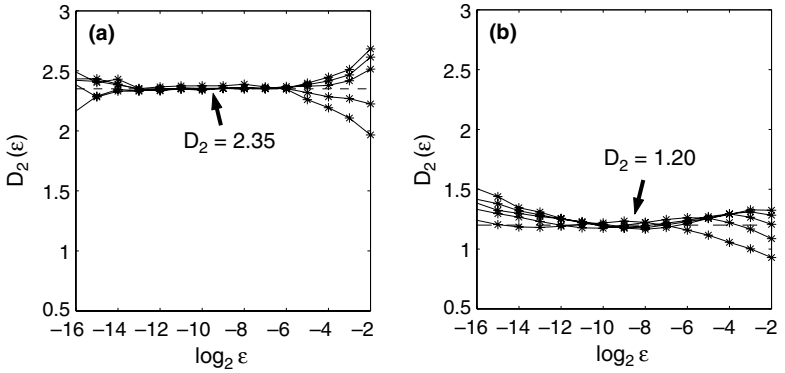

Fig. 5. The correlation dimension $D_2(\epsilon)$ vs. $\log_2\epsilon$ curves for a series of m values, $m = 12, 14, 16, 18, 20$ for (a) the $h(t)$ time series of Fig. 2(c), and (b) the $h(t)$ time series of Fig. 6(e) (re-sampled with $\delta t = 10^{-4}$). Again, L is 3 for (a) and 6 for (b), as in the calculation of the $\Lambda(k)$ curves.

will explain why we choose such a small sampling time later). Similar to the delay differential equation model, the negative value of h also means that there is contact loss between the tool and a workpiece. We observe from Fig. 6(a) that when $\omega = 800$ rad/s, the cutting process is very smooth with only negligible oscillations around h_0. The $h(t)$ time series becomes more complex as ω increases, until $\omega = 1200$ rad/s, we observe that the $h(t)$ time series appears to be weakly aperiodic. This could be caused by the loss of synchronization between impact incidents and the driving frequency ω. As ω further increases, the vibrations of the cutting depth $h(t)$ become regular again.

To better appreciate the complexity of the time series of Fig. 6, we plot the phase diagram and compute the PSD. Since the time series shown in Fig. 6(a) and (h) are simple, and the time series in Fig. 6(f) and (g) are quite similar to the time series in Fig. 6(b), so from now on, we shall focus on the time series shown in Fig. 6(b)–(e). Their corresponding phase diagram and PSD are shown in Fig. 7(a), (c), (e) and (g) and Fig. 7(b), (d), (f) and (h), respectively. The delay time for computing the phase diagram is $L = 1200$, such a large delay time is determined by the very small sampling time chosen here. We observe from Fig. 7(a) that the orbit in the phase space takes two runs until the path repeats. We also observe that the smallest spectral peak is 1/2 of the dominant peak in Fig. 7(b). Therefore, the motion for $\omega = 1120$ rad/s is period-2. Similarly, we observe from Fig. 7(c) and (d) that the motion for $\omega = 1180$ rad/s is period-4, while it is period-7 for $\omega = 1190$ rad/s. The phase diagram and the PSD for the motion for $\omega = 1200$ rad/s suggest that the time series shown in Fig. 6(e) may be chaotic. Note that the phase diagram and the PSD for the time series of Fig. 6(g) (which was analyzed by Litak) are very similar to those shown in Fig. 7(a) and (b). The many spectral peaks have motivated Litak to conjecture that the motion may be quasi-periodic. It is clear from the phase diagram and the PSD shown in Fig. 7(a) and (b) that the motion is not quasi-periodic, but period-2.

To examine whether the dynamics corresponding to $\omega = 1200$ rad/s is truly chaotic, we compute the $\Lambda(k)$ curves and calculate the correlation dimension. To facilitate comparison between the two models, we first downsample the $h(t)$ time series for $\omega = 1200$ rad/s by 100 times, thus the sampling time becomes $\delta t = 10^{-4}$. Following the optimal embedding procedure developed in [24], we find that a proper L for the downsampled time series is 6. The $\Lambda(k)$ curves are fairly independent of the embedding dimension m, so long as m is not too small. Fig. 4(b) shows one example of the $\Lambda(k)$ curves computed by Eq. (8). The four curves, from bottom to top, correspond to the shells of sizes $(2^{-(i+1)/2}, 2^{-i/2})$, $i = 12, 13, 14, 15$. We can roughly observe a common envelope at the lower left corner of Fig. 4(b). The largest positive Lyapunov exponent is found to be 80 bits per sec, or 0.420 bits per cycle of the oscillation, after being multiplied by the period of the oscillation. Note that this number is slightly smaller than 0.593, which is a typical value for the largest positive Lyapunov exponent for the chaotic motion of the delay differential equation model.

Next we calculate the correlation dimension D_2 for the time series of Fig. 6(e). The curves of $D_2(\epsilon)$ vs. $\log_2\epsilon$ for a series of m are plotted in Fig. 5(b). We observe a constant plateau, with a value of $D_2 = 1.2$. Note that this number is much smaller than the correlation dimension for the chaotic motion of the delay differential equation model.

Now, let us explain why we choose a very small sampling time for the Litak's model. The reason is that if we choose a larger sampling time, some of the details of the signals will be lost. To better appreciate the sampling time effect, let us downsample the $h(t)$ time series for $\omega = 1190$ rad/s by 100 times, thus, obtaining a new time series with a sampling time of 10^{-4}. We then plot the phase diagram (choosing $L = 12$) and the PSD for this downsampled time series, as shown in

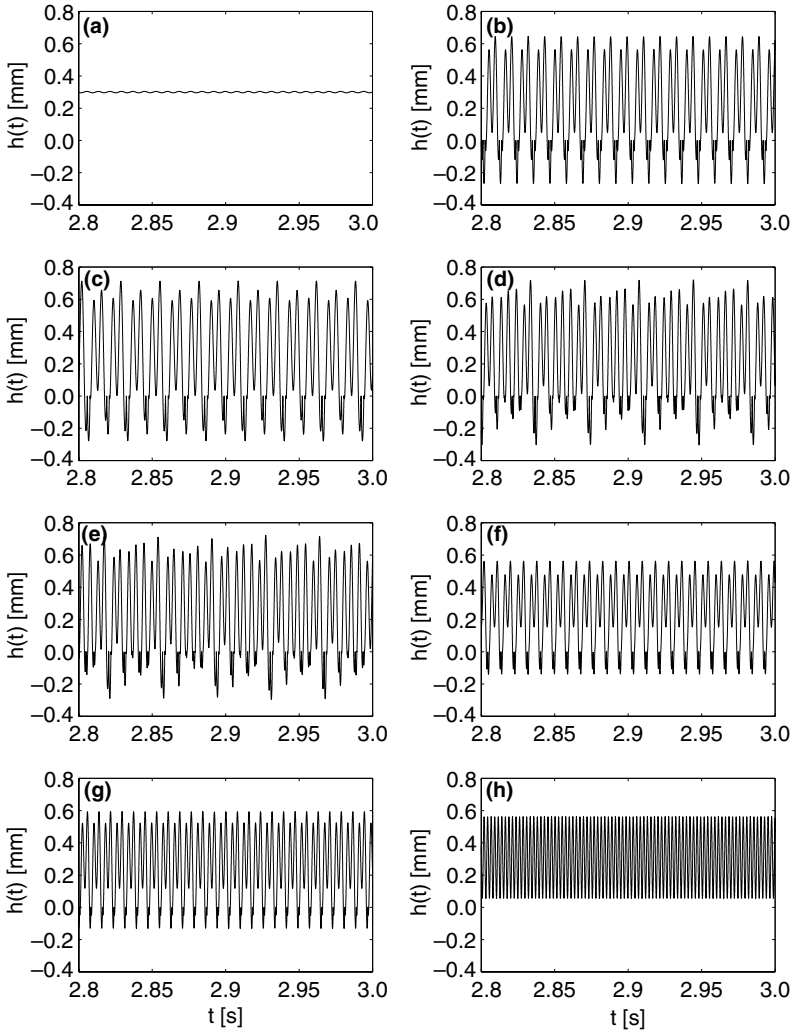

Fig. 6. The actual cutting depth $h(t)$ corresponding to various frequencies ω of the Litak's model: (a) $\omega = 800$ rad/s, (b) $\omega = 1120$ rad/s, (c) $\omega = 1180$ rad/s, (d) $\omega = 1190$ rad/s, (e) $\omega = 1200$ rad/s, (f) $\omega = 1400$ rad/s, (g) $\omega = 1600$ rad/s, (h) $\omega = 2600$ rad/s. The time series is sampled with $\delta t = 10^{-6}$.

Fig. 8(a) and (b). Note that Fig. 8(a) appears to be similar to Fig. 7(g). One thus may be tempted to interpret the motion in Fig. 8 as chaotic. Fortunately, the $\Lambda(k)$ curves for the downsampled time series for $\omega = 1190$ rad/s (Fig. 4(c)) show that the time series is not truly chaotic, but periodic. Because we observe that all the $\Lambda(k)$ curves in Fig. 4(c) are very close to 0.

Before leaving this section, we shall make a few comments on the behaviors of the two models. We observe that the $h(t)$ time series of the Litak's model [10] are much more spiky than those generated by the delay differential equation model. Why is this so? Recalling that the purpose of introducing the harmonic forcing is to replace $y(t - T)$ to simplify the delay differential equation model, we thus see that incompatibility arises when $y(t)$ and $y(t - T)$ take on entirely different functional forms, such as when $y(t)$ is chaotic. When incompatibility occurs, the signals become spiky. It appears that the Litak's model has an interesting attribute of making this incompatibility as small as possible by forcing $y(t)$ to be as close to the sinusoidal forcing as possible. Indeed, we have found that the chaotic motion from the Litak's model has sharper spectral peaks, a smaller correlation dimension and a smaller value for the largest positive Lyapunov exponent (in fact, the correlation dimension is only slightly larger than 1 for the chaotic motion generated by the Litak's model). The behavior of the Litak's model highly suggests that chaos in machine cutting processes could be greatly suppressed if one employs certain chaos control technique.

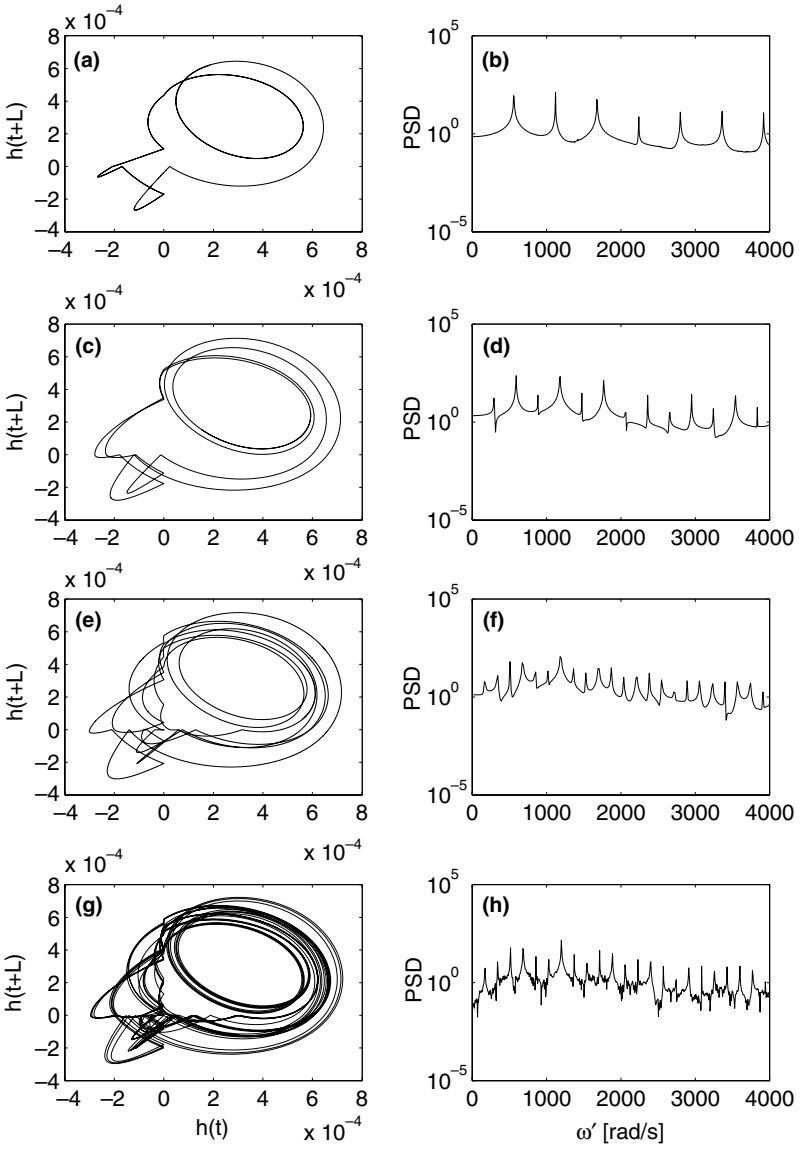

Fig. 7. The phase diagram (a), (c), (e) and (g) and PSD (b), (d), (f), and (h) for the time series of various frequencies ω of the Litak's model: (a) and (b) $\omega = 1120$ rad/s, (c) and (d) $\omega = 1180$ rad/s, (e) and (f) $\omega = 1190$ rad/s, (g) and (h) $\omega = 1200$ rad/s. The phase diagram is plotted with $L = 1200$.

3. Discussions and conclusions

In this paper, we have studied machine cutting processes by two different models, one is the classic delay differential equation model, the other has been recently introduced by Litak. We have carefully analyzed the periodic and chaotic vibrations for both models. We have not observed quasi-periodic motions from either model. While we have observed the period-doubling phenomenon in the Litak's model, the route to chaos is not via period-doubling, because period-7 oscillations are observed before chaos occurs. We have carefully compared the dynamics of the two models, and found the signals from the Litak's model are much more spiky. We have explained that the spikiness may result from the incompatibility between the sinusoidal approximation for $y(t - T)$ and the more complicated dynamics of $y(t)$. It appears that the Litak's model has an interesting attribute of making this incompatibility as small as possible. As a result, the chaotic motion from the Litak's model has sharper spectral peaks, a smaller correlation dimension and a smaller

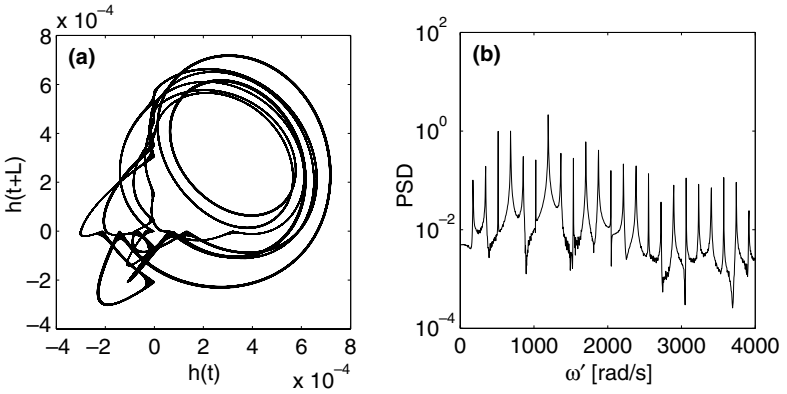

Fig. 8. The phase diagram (a) and PSD (b) for the re-sampled time series (sampled with 10^{-4}) for $\omega = 1190$ rad/s of the Litak's model. The phase diagram is plotted with $L = 12$.

value for the largest positive Lyapunov exponent. The spikiness of the signals also determines that the sampling time has to be very small, otherwise some features of the signals may get lost. While from the phase diagram of Fig. 8(a), one might be tempted to interpret the motion to be chaotic, fortunately, we have found that the $\Lambda(k)$ curves can be reliably used to show that the motion is not truly chaotic, but simply periodic, disregarding the sampling time.

The ultimate goal of studying the complex dynamics of machine cutting processes is to help design novel methods of eliminating chaos and large amplitude oscillations. The marked difference between the dynamic behaviors of the Litak's model and the delay differential equation model suggests that this goal is feasible.

Acknowledgement

X.S. Wang was partially supported by the Chinese National Scientific Foundation (Project number 50475076).

References

[1] Shi HM, Tobias SA. Theory of finite amplitude machine tool instability. Int J Mach Tool Des Res 1984;24:45–69.
[2] Wu DW, Liu CR. An analytical model of cutting dynamics. Part 1: model building. ASME J Eng Indust 1985;107:112–8.
[3] Grabec I. Chaos generated by the cutting process. Phys Lett A 1986;117:384–6.
[4] Grabec I. Chaotic dynamics of the cutting process. J Mach Tools Manufact 1988;28:19–32.
[5] Marui E, Kato S, Harashimoto M, Yamada T. The mechanism of chatter vibrations in a spindle-workpiece system: Part 2—characteristics of dynamic cutting force and vibration energy. ASME J Eng Indust 1988;110:242–7.
[6] Smith S, Tlusty J. An overview of modelling and simulation of the milling process. ASME J Eng Indust 1991;113:169–75.
[7] Gradisek J, Govekar E, Grabec I. A chaotic cutting process and determining optimal cutting parameter using neural networks. Int J Mach Tools Manufact 1996;36:1161–72.
[8] Gradisek J, Govekar E, Grabec I. Chatter onset in non-regenerative cutting: a numerical study. J of sound and vibration 2001;242:829–38.
[9] Litak G, Warminski J, Lipski J. Self-excited vibrations in cutting process. In: Awrejcewicz J, Grabski J, Mrozowski J, editors. Proceedings of 4th Conference on Dynamical Systems—Theory and Applications, 8–9 December 1997; Lodz., p. 193–7.
[10] Litak G. Chaotic vibrations in a regenerative cutting process. Chaos, Solitons & Fractals 2002;13:1531–5.
[11] Wiercigroch M. Chaotic vibrations of a simple model of the machine tool—cutting system. ASME J Vibr Acoust 1997;119:468–75.
[12] Wiercigroch M, Cheng AH-D. Chaotic and stochastic dynamics of orthogonal metal cutting. Chaos, Solitons & Fractals 1997;8:715–26.
[13] Stepan G, Kalmar-Nagy T. Nonlinear regenerative machine tool vibrations. In: Proceedings of 16th ASME Biennial Conference on Mechanical Vibrations and Noise, ASME Design and Technical Conference, 14–17 September 1997; Sacramento, CA, p. 1–11.
[14] Stepan G. Delay-differential equation models for machine tool chatter. In: Moon FC, editor. Dynamics and chaos in manufacturing processes. Wiley; 1998. p. 165–92.
[15] Stepan G. Modelling nonlinear regenerative effects in metal cutting. Phil Trans R Soc Lond A 2001;359:739–57.
[16] Nayfeh AH, Chin CM, Pratt J. Applications of perturbation methods to tool chatter dynamics. In: Moon FC, editor. Nonlinear dynamics of material processing and manufacturing. Wiley; 1997. p. 123–93.

[17] Ehmann KF, Kapoor SG, DeVor RE, Lazoglu I. Machining process modeling: a review. J Manufact Sci Eng—Trans ASME 1997;119:655–63.
[18] Nosyreva EP, Molinari A. Analysis of nonlinear vibrations in metal cutting. Int J Mech Sci 1998;40:735–48.
[19] Kalmar-Nagy T, Pratt J, Davies MA, Kennedy MD. Experimental and analytical investigation of the subcritical instability in metal cutting. In: Proceedings of 17th ASME Biennial Conference on Vibration and Noise, 1999 Las Vegas, NV, Paper no. DETC99/VIB-8060, p. 1–9.
[20] Pratt JR, Nayfeh AH. Design and modelling for chatter control. Nonlinear Dyn 1999;19:49–69.
[21] Warminski J, Litak G, Lipski J, Wiercigroch M, Cartmell MP. Vibrations in regenerative cutting process synthesis of nonlinear dynamical systems. In: Lavendelis E, Zakrzhevsky M, editors. Solid Mechanics and its Applications, 73. Dordrecht: Kluwer Academic Publishers; 2000. p. 275–83.
[22] Warminski J, Litak G, Cartmell MP, Khanin R, Wiercigroch M. Approximate analytical solutions for primary chatter in the non-linear metal cutting model. J Sound Vibr 2003;259:917–33.
[23] Fofana MS. Delay dynamical systems and applications to nonlinear machine-tool chatter. Chaos, Solitons & Fractals 2003;17:731–47.
[24] Gao JB, Zheng ZM. Local exponential divergence plot and optimal embedding of a chaotic time series. Phys Lett A 1993;181:153–8;
Gao JB, Zheng ZM. Direct dynamical test for deterministic chaos and optimal embedding of a chaotic time series. Phys Rev E 1994;49:3807–14;
Gao JB, Zheng ZM. Direct dynamical test for deterministic chaos. Europhys Lett 1994;25:485–90.
[25] Gao JB. Recognizing randomness in a time series. Physica D 1997;106:49–56;
Gao JB, Hwang SK, Liu JM. Effects of intrinsic spontaneous-emission noise on the nonlinear dynamics of an optically injected semiconductor laser. Phys Rev A 1999;59:1582–5;
Gao JB, Hwang SK, Liu JM. When can noise induce chaos? Phys Rev Lett 1999;82:1132–5;
Gao JB, Chen CC, Hwang SK, Liu JM. Noise-induced chaos. Int J Mod Phys B 1999;13:3283–305;
Hwang K, Gao JB, Liu JM. Noise-induced chaos in an optically injected semiconductor laser. Phys Rev E 2000;61:5162–70;
Gao JB, Tung WW, Rao N. Noise induced Hopf bifurcation-type sequence and transition to chaos in the Lorenz equations. Phys Rev Lett 2002;89:254101.
[26] Hu J, Gao JB, White KD. Estimating measurement noise in a time series by exploiting nonstationarity. Chaos, Solitons & Fractals 2004;22:807–19.
[27] Cellucci CJ, Albano AM, Rapp PE, Pittenger RA, Josiassen RC. Detecting noise in a time series. Chaos 1997;7:414–22.
[28] Gao JB, Yao K. Multifractal features of sea clutter. In: IEEE Radar Conference 2002, Long Beach, CA, April 2002.Gao JB, Hwang SK, Chen HF, Kang Z, Yao K, Liu JM. Can sea clutter and indoor radio propagation be modeled as strange attractors? In: The 7th experimental chaos conference, San Diego, USA, August 2002; p. 25–9.
[29] Gao JB, Tung WW. Pathological tremors as diffusional processes. Biol Cyber 2002;86:263–70.
[30] Gao JB, Rao NSV. Complicated dynamics of internet transport protocols. IEEE Commun Lett 2005;9:4–6;
Gao JB, Rao NSV, Hu J, Ai J. Quasi-periodic route to chaos in the dynamics of Internet transport protocols. Phys Rev Lett 2005;94:198702.
[31] Bandyopadhyay R, Sood AK. Chaotic dynamics in shear-thickening surfactant solutions. Europhys Lett 2001;56:447–53.
[32] Bandyopadhyay R, Basappa G, Sood AK. Observation of chaotic dynamics in dilute sheared aqueous solutions of CTAT. Phys Rev Lett 2000;84:2022–5.
[33] Venkadesan S, Valsakumar MC, Murthy KPN, Rajasekar S. Evidence for chaos in an experimental time series from serrated plastic flow. Phys Rev E 1996;54:611–6.
[34] Abarbanel HDI. Analysis of observed chaotic data. Springer; 1996.
[35] Grassberger P, Procaccia I. Characterization of strange attractors. Phys Rev Lett 1983;50:346–9.